Generation of high purity microwave signal from a dual-frequency OP-VECSEL (orale)

Fabiola Camargo, Gaëlle Lucas-Leclin, Paul Dumont, Patrick Georges, Jean-Marie Danet, David Holleville, Stéphane Guerandel, Grégoire Pillet, Ghaya Baili, Loïc Morvan, et al.

▶ **To cite this version:**

Fabiola Camargo, Gaëlle Lucas-Leclin, Paul Dumont, Patrick Georges, Jean-Marie Danet, et al.. Generation of high purity microwave signal from a dual-frequency OP-VECSEL (orale). LASE 2014 - Conference on Vertical External Cavity Surface Emitting Lasers (VECSELs) IV, Feb 2014, San Francisco, United States. pp.89660L, 10.1117/12.2041669 . hal-00959737

HAL Id: hal-00959737

https://hal-iogs.archives-ouvertes.fr/hal-00959737

Submitted on 15 Mar 2014

HAL is a multi-disciplinary open access archive for the deposit and dissemination of scientific research documents, whether they are published or not. The documents may come from teaching and research institutions in France or abroad, or from public or private research centers.

L'archive ouverte pluridisciplinaire **HAL**, est destinée au dépôt et à la diffusion de documents scientifiques de niveau recherche, publiés ou non, émanant des établissements d'enseignement et de recherche français ou étrangers, des laboratoires publics ou privés.

Generation of high purity microwave signal from a dual-frequency OP-VECSEL

Fabiola Camargo[a], Gaëlle Lucas-Leclin[a] Paul Dumont[a], Patrick Georges[a], Jean-Marie Danet[b], David Holleville[b], Stéphane Guerandel[b], Grégoire Pillet [c], Ghaya Baili [c], Loïc Morvan [c], Daniel Dolfi [c], Iryna Gozhyk [d], Grégoire Beaudoin [d], Isabelle Sagnes[d]

[(a)] Laboratoire Charles Fabry, Institut d'Optique, CNRS, Univ Paris-Sud 11, Palaiseau, France
[(b)] LNE-SYRTE, Systèmes de Référence Temps-Espace, Observatoire de Paris, CNRS, UPMC, Paris, France
[(c)] Thales Research & Technology, Palaiseau, France
[(d)] Laboratoire de Photonique et de Nanostructures, CNRS UPR20, Marcoussis, France

ABSTRACT

Coherent population trapping (CPT) is an interesting technique for the development of compact atomic frequency references. We describe an innovating laser source for the production of the two cross-polarized coherent laser fields which are necessary in CPT-based atomic clocks. It relies on the dual-frequency and dual-polarization operation of an optically-pumped vertical external-cavity semiconductor laser. This particular laser emission is induced by intracavity birefringent components which produce a controllable phase anisotropy within the laser cavity and force emission on two cross-polarized longitudinal modes. The laser emission is tuned at the Cs D_2 line (λ = 852.14 nm), and the frequency difference $\Delta\nu$ between the two laser modes is tunable in the microwave range.
The laser line wavelength is stabilized onto an atomic hyperfine transition, and concurrently the frequency difference is locked to an ultra-low noise RF oscillator at 9.2 GHz. The high spectral purity of the optically-carried microwave signal resulting from the beatnote of the two cross-polarized laser lines is assessed through its narrow spectral linewidth (<30 Hz) as well as its low phase noise ($\leq$ -100 dBrad^2/Hz). The performance of this laser source is already adequate for the interrogation of atoms in a CPT atomic clock, and should result in an estimated relative stability of $3.10^{-13}\tau^{-1/2}$ – one order of magnitude better than commercial atomic clocks.

Keywords: Vertical External Cavity Surface-Emitting Lasers, Atomic Clocks, Metrology, Microwave Photonics.

1. INTRODUCTION

Microwave photonics is an emerging field which studies the generation, distribution, processing and analysis of microwave signals carried on optical frequency carriers, using the advantages of photonics technologies [1,2]. It enables access to high-frequency signals generation and processing, without the state-of-the-art electronics and also to long range transmission of microwave signals through optical fiber links. Firstly developed for defense applications, microwave photonics spreads to a large number of civil applications such as cellular, wireless, and satellite communications and medical imaging. It is also used in metrology, in the development of frequency standards and inertial captors.

Here we are interested in the realization of compact and stable atomic clocks using the coherent population trapping (CPT) phenomenon in which the radiofrequency (RF) probe frequency is optically carried [3,4]. More precisely, in a CPT-based atomic clock, the microwave interrogation that delivers the atomic reference signal is induced by two phase-coherent laser fields at resonance with a common excited state. When the frequency difference between the two laser fields corresponds exactly to the ground-state hyperfine splitting (equal to 9.192 631 770 GHz with Cs atoms), the atoms are trapped in a dark state and stop interacting with the laser light. The resulting narrow transmission line in the atomic absorption spectrum is used as a frequency reference. In order to guarantee the stability of the clock frequency, CPT atomic clocks require a high purity, optically carried, microwave signal as well as low-noise properties for the laser source (intensity and frequency fluctuations). Among the different optical configurations which influence the CPT signal, those combining cross-polarized excitation scheme and temporal Ramsey-like pulsed interrogation have

demonstrated highly contrasted and narrow-linewidth CPT resonance [5]. Such configuration was recently proven to reach short-term frequency stability of 3.2 × 10-13 $\tau^{-1/2}$[6].

The common solution for the production of the coherent pair of laser beams in such a polarization configuration is the optical phase-locking of two independent lasers. However, as miniaturization is a challenge for such clocks, a simplified optical bench using a single laser source would be a serious improvement for CPT clocks. Recently, the dual-frequency emission of a solid-state laser has been demonstrated in the GHz range with a Er:Yb:Glass laser [7] and a Nd:YAG laser [8], both based on the simultaneous emission of two cross-polarized longitudinal modes inside the same laser cavity. However, the main limitation of these lasers is their strong intensity noise inherent to their class-B dynamical behavior. In order to overcome this limitation, dual-frequency emission has been demonstrated in a class A optically pumped vertical-external-cavity semiconductor laser (OP-VECSEL) which does not suffer from relaxation oscillation since the photon lifetime inside the cavity is much longer than the excited carriers lifetime. This configuration has been demonstrated at 1 µm [9] and 852 nm [10].

2. DESIGN AND OPERATION OF THE DUAL-FREQUENCY AND DUAL-POLARIZATION OP-VECSEL

The optically-pumped VECSEL design enables the introduction of free-space intracavity elements to force the dual-frequency and dual-polarization emission of the cavity, while using specially designed semiconductor structure emitting at the targeted wavelength [11].

2.1. Semiconductor structure

The semiconductor chip is a conventional multilayer active structure, grown with metal-organic chemical-vapor deposition on a 350 µm-thick GaAs substrate. A distributed Bragg reflector (DBR), composed of 32.5 pairs of λ/4-thick AlAs/$Al_{0.225}Ga_{0.775}As$ layers, provides a 80-nm large high reflectivity centered at 850 nm, with R > 99.94% at 852 nm. The 30 λ/4-thick active structure is composed of seven 8 nm-thick GaAs quantum wells (QW) embedded in pump-absorbing $Al_{0.225}Ga_{0.775}As$ barriers; the QW are positioned at the antinodes of the optical standing wave following a 11110101001000 sequence (starting at the air surface, see Figure 1) resulting in almost identical pumping for each QW. The pump absorption is 90 % of the internal pump power in a single pass. Two 30-nm thick $Al_{0.39}Ga_{0.61}As$ layers form potential barriers on each side of the active cavity, for carrier confinement. Finally, a 50 nm-thick InGaP capping layer protects the cavity from Al-oxidation. The design of this structure, without anti-reflection coating, results in an enhancement of the modal gain by a factor of 3 thanks to constructive interferences inside the semiconductor sub-cavity.

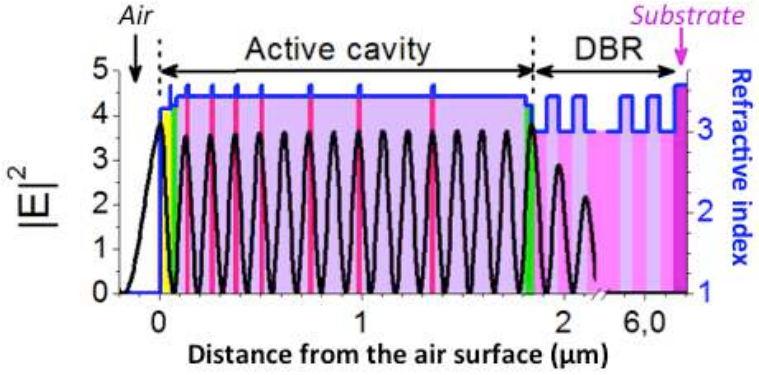

Figure 1. Description of the semiconductor active chip; (black line, left axis) intensity of the resonant field at λ = 850 nm; (blue line, right axis) refractive index.

2.2. Laser cavity

The laser cavity is composed of the semiconductor chip and a R = 15 mm concave output coupler, transmitting 0.5 % at 850 nm. The pump source is a broad-area laser diode emitting at 670 nm, coupled into a 100 µm diameter, NA = 0.22, multimode fiber. This source delivers up to 1 W at the fiber end. The pump beam is focused on the semiconductor chip with two doublets (f_1 = 25 mm, f_2 = 19 mm) under a 50° angle, yielding a 70 µm by 110 µm-elliptical spot on the semiconductor structure. About 30% of the incident pump power is reflected onto the surface.

The dual-polarization emission is obtained by introducing a birefringent element in the laser cavity, which raises the degeneracy between polarizations and thus results in the stable oscillation of two cross-polarized modes. Here we use a

500 µm-thick antireflection coated YVO_4 plate cut at 45° to its optical axis, which induces a spatial separation d of 50 µm between the extraordinary and ordinary beams in the structure along the longer axis of the pump ellipse (Figure 2). This spatial separation reduces the coupling between the two polarizations which ensures the stable dual-polarization, dual-frequency emission [12]; nevertheless the spatial separation is small enough to maintain a good overlap between the pump beam and the two laser spots. Finally, the single-frequency operation at each polarization, as well as the wavelength coarse tunability, are obtained using a 50 µm-thick uncoated silica etalon with a free spectral range FSR_{Etalon} = 2 THz. Fine tuning of the laser wavelength is obtained using a piezo-transducer glued on the output coupler. To control the laser frequency difference, a 5 % MgO-doped stoichiometric lithium tantalate (SLT) crystal is placed within the cavity. Its high transparency at 852 nm minimizes additional intra-cavity losses. The crystal axes are oriented to limit the ordinary-polarized mode frequency dependency with the SLT applied voltage. With all intra-cavity elements, the FSR of the laser cavity is FSR_{cav} = 12 GHz, higher than the targeted frequency difference $\Delta\nu_{Cs}$ = 9.192 GHz, and corresponding to an optical cavity length L_{cav} = 12.5 mm.

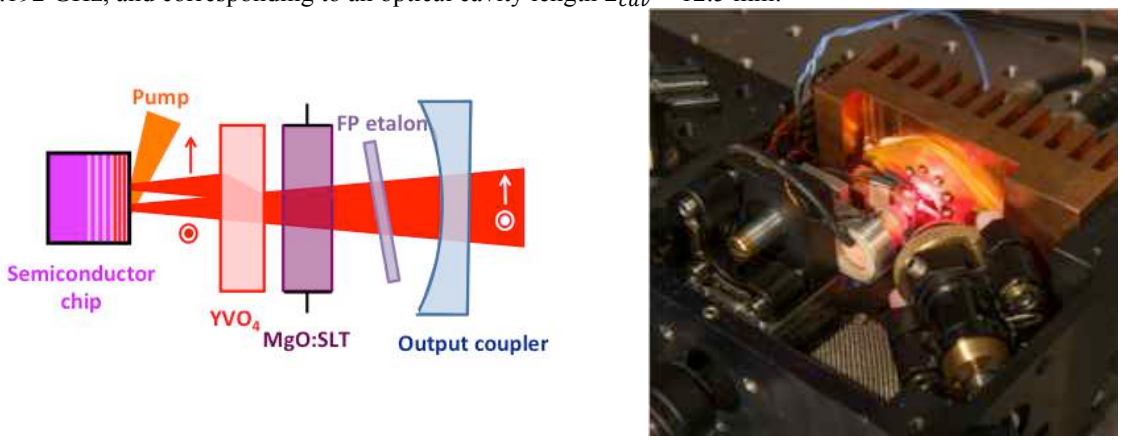

Figure 2. (left) scheme of the laser setup; (right) photograph of the dual-frequency laser prototype.

The laser cavity design has focused on compactness as well as high mechanical and thermal stability. The pump optics, the semiconductor chip and the intra-cavity elements are integrated in a compact 90 mm × 90 mm × 40 mm casing (see Figure 2). This limits mechanical and acoustic vibrations as well as air temperature fluctuations inside the external cavity. The temperature of the whole set-up is stabilized to 24°C. The semiconductor chip temperature is maintained at 16°C using a Peltier element, and the SLT crystal and YVO_4 plate are fixed on the same temperature-controlled copper mount.

2.3. Frequency difference tunability

The birefringence introduced inside the cavity generates two combs of cross-polarized longitudinal modes. For two adjacent cross-polarized oscillating modes (i.e. with a frequency difference below FSR_{cav}), the laser beatnote frequency, defined as the frequency difference $\Delta\nu = |\nu_{ext} - \nu_{ord}|$, is given by the formula:

$$\Delta\nu = \mathrm{FSR_{cav}}\left|\frac{2\Delta L}{\lambda}\right| \quad (1)$$

where $\Delta L = L_{cav}^{ext} - L_{cav}^{ord}$ corresponds to the optical path difference due to the birefringence inside the cavity, and is defined modulo $\lambda/2$. Thus $\Delta\nu$ is tunable over one FSR of the cavity. The tunability of ΔL is calculated from the contributions of both YVO_4 and SLT crystals, taking into account three main effects: thermal expansion, thermo-optic and electro-optic effects. The birefringence variation of SLT with the applied transverse voltage follows the relationship:

$$\Delta n_{SLT}^{EO}(V) = \frac{V}{e}\left(\frac{n_e^3}{2}r_{33} - \frac{n_o^3}{2}r_{13}\right) \quad (2)$$

where e = 2 mm is the distance between the two electrodes used to apply a voltage V on the crystal, n_e and n_o are the refraction indexes for the extraordinary and ordinary polarizations, r_{33} and r_{13} are the electro-optic coefficients along the axes x and z, respectively (x is the axis on which the voltage is applied and z is along the beam propagation). The contribution of thermal changes on birefringence can be estimated with the following relationship:

$$\frac{\partial(\Delta L)}{\partial T} = \frac{\partial L}{\partial T}(n_e - n_o) + L\left(\frac{\partial n_e}{\partial T} - \frac{\partial n_o}{\partial T}\right) \quad (3)$$

and using the thermal expansion coefficients $\alpha = \frac{\partial L}{\partial T}\frac{1}{L}$ and the thermo-optic coefficients β_e, $\beta_o = \frac{\partial n}{\partial T}\frac{1}{n} = \sum a_i T^i$ for the ordinary and extraordinary polarizations.

Table 1. Material parameters of YVO_4 crystal at 25°C by Ter-Gabrielyan & al. [13]

YVO_4 material parameters at 25°C		
Refractive index at 852 nm	$n_o = 1.9702$	$n_e = 2.1811$
Thermo-optic coefficients (K^{-1})	$a_0 = -3.67 \times 10^{-6}$ $a_1 = 9.79 \times 10^{-8}$ $a_2 = -1.13 \times 10^{-10}$	$a_0 = 8.07 \times 10^{-7}$ $a_1 = 2{,}89 \times 10^{-8}$
Thermal expansion coefficient (K^{-1})	$\alpha_\perp = 2.06 \times 10^{-6}$	$\alpha_\parallel = 8.44 \times 10^{-6}$

Table 2. Material parameters of SLT crystal doped with MgO at 25°C by Dolev & al. [14]

MgO-doped SLT material parameters		
Refractive index at 852 nm	$n_o = 2.1441$	$n_e = 2.1418$
Thermo-optic coefficients (K^{-1})	$a_0 = 5.586 \times 10^{-5}$ $a_1 = 0.92168 \times 10^{-8}$	$a_0 = 1.8017 \times 10^{-5}$ $a_1 = 6.1500 \times 10^{-8}$
Thermal expansion coefficient (K^{-1})	$\alpha_\perp = 1.5 \times 10^{-5}$	unknown
Electro-optic coefficient (pm/V)	$r_{13} = 6.96$	$r_{33} = 29.6$

From material parameters values in Tables 1 & 2, we compute the sensitivity of the frequency difference $\Delta\nu$ to temperature and to EO applied voltage of, respectively, 1.41 GHz/K at 25°C and 1.56 MHz/V. Thus the crystal temperature allows a coarse tunability of the frequency difference to the targeted value of 9.192 GHz.

2.4. Laser characterization

Without intra-cavity elements, the laser threshold is obtained at 0.25 W of incident pump power. The laser output power reaches 83 mW for the maximal pump power limited by thermal effects in the semiconductor structure; the laser emission exhibits then a multimode spectrum centered at 855 nm. With the Fabry-Perot etalon, the laser operates in single mode emission with a wavelength tunability of almost 5 nm.

With all intra-cavity elements, the laser threshold increases to 0.35 W and the laser output power decreases to 26 mW at 852.1 nm - corresponding to 13 mW per polarization. The fine tunability of the cross-polarized laser lines is achieved with the rotation of the Fabry-Perot etalon and the adjustment of the cavity length. Proper adjustments of the cavity and pump alignments allows to force the laser emission on two adjacent longitudinal modes on orthogonal polarizations, with a frequency difference $\Delta\nu$ below the free-spectral range of the cavity. The beatnote frequency is evidenced by mixing the cross-polarized modes with a polarizer oriented at 45° of their axes, and coupling the beam into a fiber-coupled fast photodiode followed by two low-noise RF amplifiers (Gain = 22 dB each) and a RF amplifier. The generated beatnote frequency is around 9.2 GHz with a spectral linewidth at -3 dB below 600 kHz on a time scale of 300 ms, measured with a resolution bandwidth of 100 kHz (Figure. 3). The tunability of the frequency difference is 1.4 GHz/K with the temperature of the SLT and YVO_4 crystals, and 1.3 MHz/V with the voltage applied to the SLT crystal – in good agreement with our numerical estimation in §2.3.

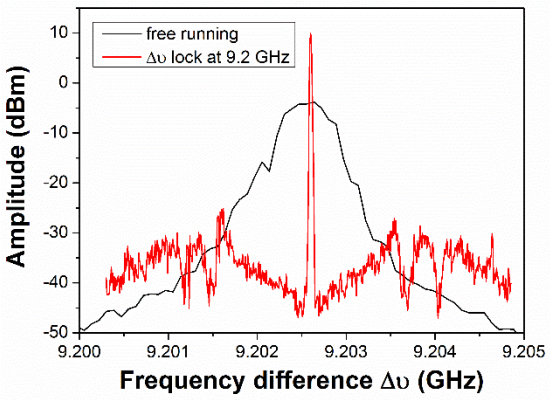

Figure 3. Beatnote frequency spectrum in free-running operation (RBW = 100 kHz) and in lock operation (RBW = 10 kHz), at 9.2 GHz. Noise is rejected 1 MHz away from the carrier frequency.

3. LASER STABILIZATION

Under free-running conditions, the laser performance is not compatible with the interrogation of Cs atoms in a CPT-based atomic clock, which requires a high-purity optically-carried microwave signal. Thus the laser emission has to be further stabilized. In this section we detail the stabilization of the ordinary-polarized laser line onto a hyperfine Cs atomic transition, and the concurrent locking of the frequency difference onto a RF oscillator.

At the output of the laser, the two cross-polarized modes are separated by a polarization beam splitter (see Figure 4). The laser is protected from any optical feedback with two -30 dB optical Faraday isolators (one per polarization). A fraction (0.5 mW) of the ordinary-polarized power is injected into a saturated absorption set-up for its stabilization on a Cs atomic transition at 852.1 nm. Finally, both beams are recombined with the same polarization axis in order to measure the beatnote frequency and lock it on the RF frequency reference.

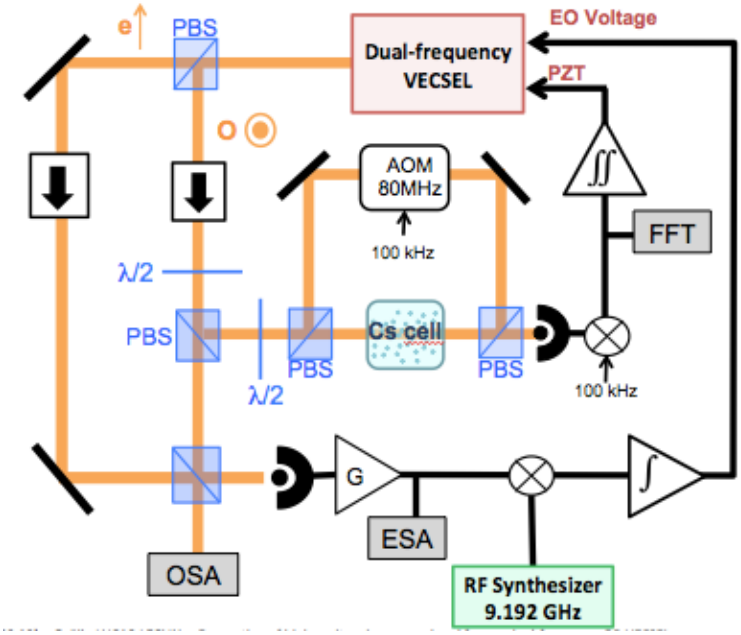

Figure 4. Stabilization set-up; EO: electro-optic crystal, PZT: piezo-electric transducer, PBS: polarization beam splitter, AOM: acousto-optic modulator, OSA: optical spectrum analyser, ESA: electrical spectrum analyzer, FFT : Fast Fourier Transform spectrum analyzer.

3.1. Optical frequency stabilization at Cs transition

The laser frequency of the ordinary polarized beam is locked onto a Doppler-free transition (F = 4 towards F' = 4'/5') of the Cs D_2 line using a pump-probe saturated absorption technique, as shown in Figure 4. An acousto-optic crystal is used to modulate the so-called pump beam at 100 kHz to generate an error signal ϵ_1. This method avoids the direct modulation of the pump diode current, which would simultaneously introduce a modulation of the laser power. The error signal is null at the top of each atomic transition, and its slope is 12 MHz/V (Figure 5). It is integrated and the correction is made by a low-frequency two-integration stages servo loop on the piezo-electric transducer glued to the output coupler.

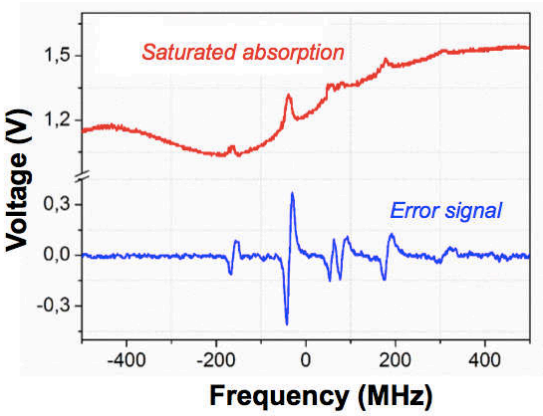

Figure 5. Saturated absorption spectrum (top) and resulting error signal (bottom)

3.2. Frequency difference stabilization

The frequency difference between the two laser modes (the so-called beatnote frequency) is locked onto a RF synthesizer, which generates a stable RF reference at the frequency ν_{RF}, using an optical phase-lock loop described in this section. After recombining the beams and superimposed their polarization axes, the two laser frequencies are mixed on a fast GaAs photodiode (Figure 4). The subsequent beatnote signal is :

$$s_{\text{beatnote}}(t) = A \sin\left(2\pi[\nu_2 - \nu_1]t + \phi_0 + \phi_{\text{RF}}(t)\right) \quad (4)$$

with ϕ_0 a constant phase term and $\phi_{\text{RF}}(t)$ the residual phase-noise fluctuations.

The beatnote signal is then amplified and mixed with the RF reference to generate an error signal ϵ_2 proportional to $(\Delta\nu - \nu_{RF})$. The error signal is then amplified by a high-bandwidth proportional-integrator corrector and applied to the intracavity electro-optic crystal to compensate for the frequency-difference fluctuations. Figure 3 compares the beatnote spectra of the free-running laser and of the laser when the frequency difference $\Delta\nu = \nu_2 - \nu_1$ is locked to the RF reference at 9.2 GHz. The linewidth of the beatnote spectrum is dramatically narrowed, below the RF analyzer resolution of 30 kHz, which evidences correction of the uncorrelated frequency fluctuations. The servo loop bandwidth is about 1 MHz, which depends on the proportional gain as well as on the electro-optic crystal response. The signal-to-noise ratio, measured between maximum of the peak and the minimum close the frequency carrier, is 55 dB.

The two servo-loops – of the absolute frequency difference on a Cs atomic transition and of the frequency difference on the RF local oscillator – operate together for 30 minutes under laboratory conditions.

4. LASER NOISE AND DYNAMICS

The noise properties of the stabilized laser emission are investigated in order to evaluate the contribution of the dual frequency OP-VECSEL to the performance of a CPT-Ramsey atomic clock. We study three main noise sources: the laser frequency noise, the beatnote phase noise and the laser intensity noise.

4.1. Laser frequency noise

The laser frequency noise reveals the fluctuations of the absolute optical frequency as compared to the Cs transition. It affects the atomic clock by reducing the interaction between Cs atoms and the laser beams. To quantify this frequency

noise, we measure the power spectral density of the error signal ϵ_1 with a Fast Fourier Transform analyzer, and normalized it by the sensitivity coefficient of the set-up (12 MHz/V). When the optical frequency locking is activated, we observed a (in-loop) noise level below the detection noise floor, meaning we reach a 60 dB frequency noise reduction at 1 Hz. The low-frequency technical noise is suppressed on a bandwidth of 300 Hz, which is limited by the piezo transducer resonance (Figure 6).

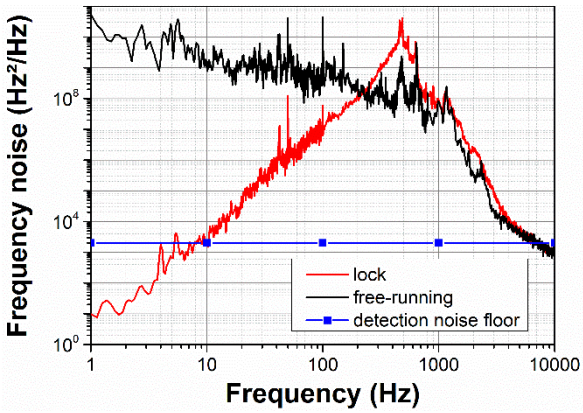

Figure 6. Power spectrum density of the frequency noise of the ordinary polarized mode, under free-running operation and under locked operation.

4.2. Beatnote phase noise

The local oscillator (LO) which provides the RF interrogation signal is a key element in an atomic frequency reference. In CPT atomic clocks, the LO frequency is optically carried for the atom interrogation process. Conversion from electrical to optical domain is obtained by locking the laser frequency difference $\Delta\nu$ to the LO frequency. This conversion may add some noise, originating from the RF synthesizer (LO), the phase-lock loop and the laser itself. To characterize the additive phase noise $\phi_{RF}(t)$ induced on the beatnote signal by the laser and the phase-lock loop, we measure the beatnote signal in an independent setup (photodiode + gain) and compare it to the RF reference (Figure 7): then the LO noise is rejected as a common contribution in the phase noise measurement.

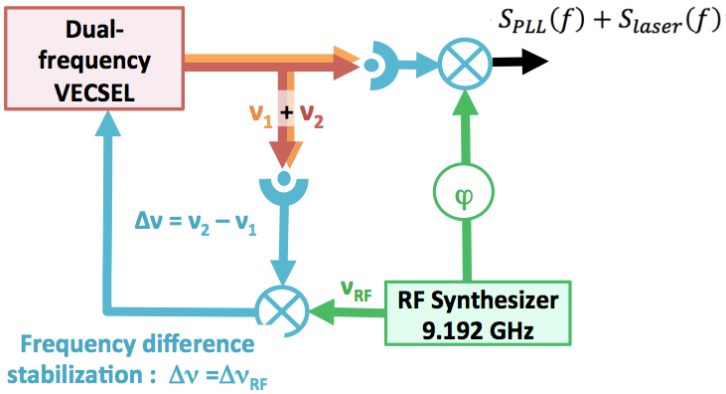

Figure 7. Additive phase noise measurements set-up. LO

Figure 8 shows the additive phase noise under free running operation and locked operation (for a frequency difference $\Delta\nu$ locked at the reference frequency of 9.6 GHz). Under free-running operation, we believe that the phase noise results mainly from the partially uncorrelated pump-induced thermal fluctuations of the semiconductor chip on each laser beam. With the phase-lock loop, the phase noise level is -105 dBrad²/Hz, below the LO standard phase noise, leading to a 100 dB noise reduction of the beatnote phase noise at 100 Hz, compared to the free running operation. At frequencies above 5 kHz, the noise level reaches -90 dBrad²/Hz up to 1 MHz which corresponds to the optical phase-lock loop bandwidth.

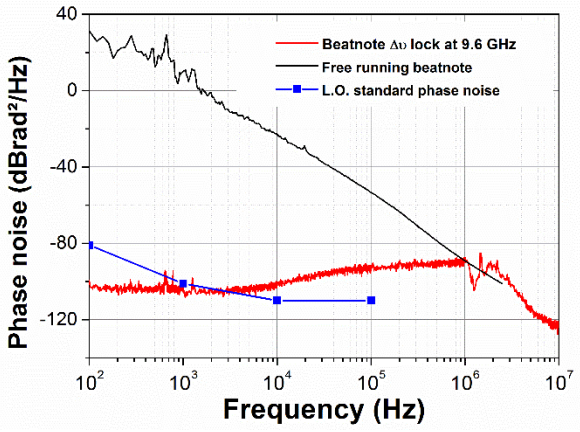

Figure 8. Power spectrum density of the beatnote phase noise due to the laser contribution under free-running operation and under locked operation (LO frequency: 9.6 GHz) compared to the standard phase noise of the LO.

4.3. Laser intensity noise

The relative intensity noise (RIN), which is converted into a frequency noise in the phase-lock loop, has been the object of a specific study. A white noise floor of -115 dB/Hz for each polarization has been measured directly at the laser output. Polarization resolved measurements show no difference of the RIN behaviour between the two modes. Moreover, the two frequency-stabilization servo-loops do not disturb the RIN level (Figure 9). The laser intensity noise is limited by the pump intensity noise with a gain factor of +5 dB consistent with theoretical estimation under our operating conditions [15]. We have verified that the RIN of the pump diode is not limited by its injected current noise, and we suspect the mode partition noise resulting from the competition between laser modes to be the main limiting factor of the pump source RIN.

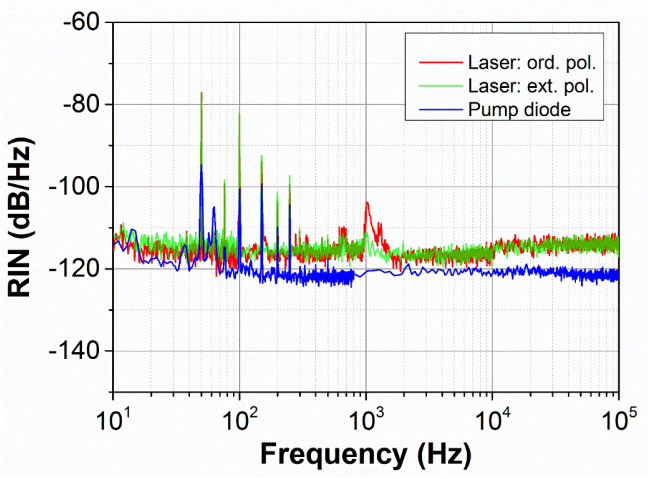

Figure 9. Spectral density of the laser relative intensity noise for each polarization, and of the pump relative intensity noise.

5. EVALUATION OF CLOCK FREQUENCY STABILITY

In this section, we evaluate the laser noise contribution to the atomic clock performance and therefore the ultimate clock frequency stability reachable with a CPT-Ramsey atomic clock using our dual frequency laser source. The atomic clock set-up is described in Figure 10. The two cross-polarized laser modes, stabilized on Cs transition lines (852 nm and with a frequency difference of $\Delta\nu$ = 9.2 GHz), illuminate a cell full of Cs atoms. An acousto-optic modulator is used for temporal pulse shaping. The clock configuration is detailed in [6]. The clock sequence of duration T_c = 6 ms is composed of a first pumping pulse τ_p = 2 ms, a free evolution time T_R = 4 ms and finally a very short detection pulse τ_d = 25 µs, during which the transmitted power through the cell is measured with a photodiode.

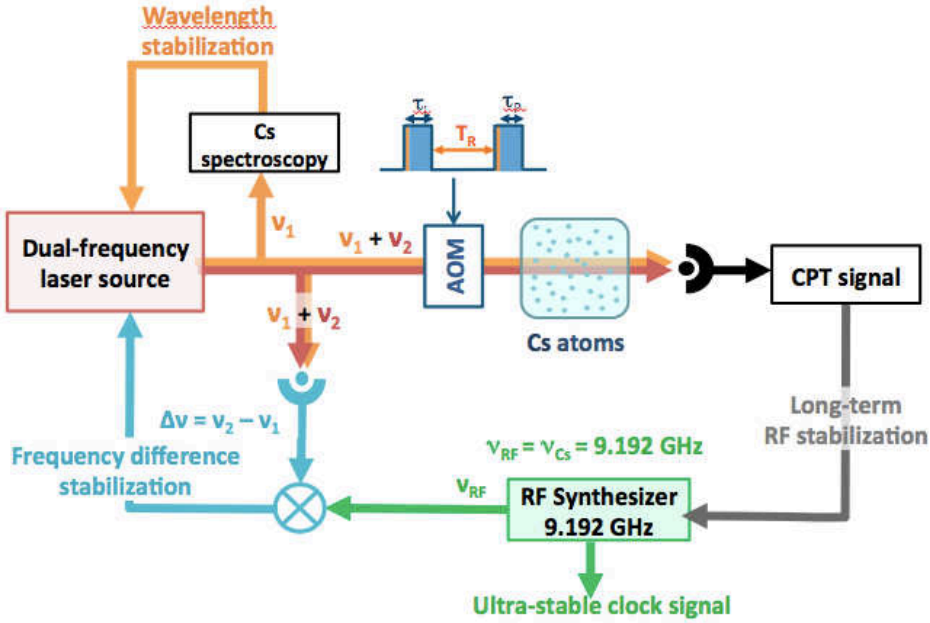

Figure 10. Scheme of the CPT atomic clock based on the dual-frequency laser source, with the three servo-loops (of the optical frequency, the frequency difference and the RF reference).

The clock frequency $\nu(t)$ is defined as the following:

$$\nu(t) = \nu_{Cs}[1 + \varepsilon + y(t)] \tag{5}$$

where ν_{Cs} is the ground-state splitting, ε the inaccuracy caused by deterministic effects, and $y(t)$ the frequency stability which corresponds to the relative frequency fluctuations of the clock signal measured on a duration time τ. To characterize the frequency stability of the signal $\nu(t)$, Allan variance is commonly used and is defined as:

$$\sigma_y^2(\tau) = \frac{1}{2}\langle(\overline{y_{k+1}} - \overline{y_k})^2\rangle \tag{6}$$

where $\overline{y_k}$ is the average value of $y(t)$ on a time interval $[t_k; t_{k+1}]$ of duration τ. $\sigma_y(\tau)$ is given by the quadratic average of three contributions: the laser intensity noise (IN), the laser frequency noise (FN) and the beatnote phase noise amplified by the Dick effect [6].

$$\sigma_y^2(\tau) = \sigma_{y/IN}^2 + \sigma_{y/FN}^2 + \sigma_{y/Dick}^2 \tag{7}$$

The major contribution of the laser power fluctuations (IN) is on the amplitude noise of the detected signal $S(t)$ which is converted into an additional clock frequency noise through the LO lock loop. Since the signal $S(t)$ is measured during a time τ_d = 25 µs, the atomic clock is sensitive to the laser intensity noise on a bandwidth of $1/\tau_d$ = 40 kHz. The clock frequency is sensitive to the laser frequency fluctuations (FN) during the pumping time τ_p of the Cs atoms. A laser frequency variation from the Cs optical transition reduces the interaction between light and atoms. Thus it induces a fluctuation of the number of atoms trapped into the dark-state, converted into amplitude noise on signal $S(t)$. The calculated sensitivity bandwidth is about 700 Hz under usual operating conditions. Finally, the Dick effect arises from the lack of information on the probe frequency during the pumping of the Cs atoms, equivalent to a dead time during which the LO noise is not probed and then not corrected [16]. It can be described by the down-conversion of the LO frequency noise at Fourier frequencies higher than the interrogation frequency. The LO frequency noise originates from its intrinsic noise and the laser beatnote frequency noise, i.e. the beatnote phase noise evaluated previously. The LO intrinsic noise will not be considered here, as we are only interested here in the noise added by the bifrequency laser source.

Table 3: Calculations of Allan variance for each laser noise contributions

Parameter	Maximum Noise Level	Allan Variance $\sigma_y(\tau)$
Laser intensity noise	-110 dB/Hz	$1.5 \times 10^{-12}\ \tau^{-1/2}$
Beatnote phase noise	-90 dBrad²/Hz	$2.7 \times 10^{-13}\ \tau^{-1/2}$
Laser frequency noise	10^{10} Hz²/Hz	$7.7 \times 10^{-14}\ \tau^{-1/2}$

The contributions to the Allan variance of the clock signal are grouped in Table 3. White noise assumption is made to simplify calculations, at the maximum measured levels. From these calculations, we estimate a clock stability of $\sigma_y(\tau) = 1.5 \times 10^{-12}\ \tau^{-1/2}$, limited by the laser intensity noise. In order to improve the short-term stability of the clock frequency, it would thus be necessary to normalize the CPT signal with the instantaneous laser power, by monitoring the laser beam power in front of the atomic cell. This technique has already been applied to CPT atomic clocks and a RIN contribution reduced at the level of $2\times10^{-13}\ \tau^{-1/2}$ seems realistic [6]. With a further improvement of the phase-lock loop to reduce the phase-noise level on the whole servo-loop bandwidth, a short-term stability of the clock frequency in the range of $3 \times 10^{-13}\ \tau^{-1/2}$ is a reasonable target.

6. CONCLUSION

The dual-frequency emission of an optically-pumped VECSEL has been demonstrated at 852 nm with a frequency difference of 9.2 GHz. Stabilized operation of the laser with both servo-loops activated has been demonstrated. Under this working operation, the laser noise properties have been carefully investigated. Numerical evaluations based on measurements of the frequency noise, the intensity noise and the beatnote phase noise, demonstrate that a clock frequency stability of 2.7 x 10^{-12} on 1 s may be achieved, limited by the intensity noise contribution. Assuming that we reduce the laser intensity noise contribution by changing either the clock or the laser set-up, the laser contribution to clock frequency stability would be limited by the Dick effect and could be reduced below 3 x 10^{-13}, paving the way for future compact atomic clocks with 1.10^{-13} frequency stability level.

ACKNOWLEDGMENTS

Part of this work was funded by the French Agence Nationale de la Recherche [ANR-07-BLAN-0320-03]. The authors gratefully aknowledge support by Triangle de la Physique [2010-089T]; the Délégation Générale de l'Armement; the Labex First-TF.

REFERENCES

1. J. Yao, "A Tutorial on Microwave Photonics," *IEEE Photonics Soc. Newsl.*, pp. 4–12, 2012.
2. D. Marpaung and C. Roeloffzen, "Integrated microwave photonics," *Laser Photon. Rev.*, pp. 1–30, 2013.
3. J. Vanier, "Atomic clocks based on coherent population trapping: a review," *Appl. Phys. B*, vol. 81, no. 4, pp. 421–442, Jul. 2005.
4. S. Knappe, V. Shah, P. D. D. Schwindt, L. Hollberg, J. Kitching, L.-A. Liew, and J. Moreland, "A microfabricated atomic clock," *Appl. Phys. Lett.*, vol. 85, no. 9, pp. 1460–1462, 2004.
5. T. Zanon, S. Guerandel, E. de Clercq, D. Holleville, N. Dimarcq, and A. Clairon, "High contrast Ramsey fringes with coherent-population-trapping pulses in a double lambda atomic system.," *Phys. Rev. Lett.*, vol. 94, no. 19, p. 193002, May 2005.
6. J. Danet, M. Lours, S. Guérandel, and E. de Clercq, "Dick effect in a pulsed atomic clock using coherent population trapping" , to be published in *IEEE Ultrason. Ferroelectr. Freq. Control*, 2014.
7. G. Pillet, L. Morvan, M. Brunel, F. Bretenaker, D. Dolfi, M. Vallet, J. P. Huignard, A. Le Floch, and S. Member, "Dual-Frequency Laser at 1.5 μm for Optical Distribution and Generation of High-Purity Microwave Signals," *J. Light. Technol.*, vol. 26, no. 15, pp. 2764–2773, 2008.
8. J. Le Gouët, L. Morvan, M. Alouini, J. Bourderionnet, D. Dolfi, and J.-P. Huignard, "Dual-frequency single-axis laser using a lead lanthanum zirconate tantalate (PLZT) birefringent etalon for millimeter wave generation: beyond the standard limit of tunability.," *Opt. Lett.*, vol. 32, no. 9, pp. 1090–2, May 2007.
9. G. Baili, L. Morvan, M. Alouini, D. Dolfi, F. Bretenaker, I. Sagnes, and A. Garnache, "Experimental demonstration of a tunable dual-frequency semiconductor laser free of relaxation oscillations.," *Opt. Lett.*, vol. 34, no. 21, pp. 3421–3, Nov. 2009.

10. F. A. Camargo, J. Barrientos, G. Baili, L. Morvan, D. Dolfi, D. Holleville, S. Guerandel, I. Sagnes, P. Georges, and G. Lucas-Leclin, "Coherent Dual-Frequency Emission of a Vertical External-Cavity Semiconductor Laser at the Cesium D2 Line," *IEEE Photonics Technol. Lett.*, vol. 24, no. 14, pp. 1218–1220, 2012.
11. O. G. Okhotnikov, *Semiconductor Disk Lasers: Physics and Technology*. ed. Wiley - VCH 2010.
12. V. Pal, P. Trofimoff, B.-X. Miranda, G. Baili, M. Alouini, L. Morvan, D. Dolfi, F. Goldfarb, I. Sagnes, R. Ghosh, and F. Bretenaker, "Measurement of the coupling constant in a two-frequency VECSEL.," *Opt. Express*, vol. 18, no. 5, pp. 5008–5014, Mar. 2010.
13. N. Ter-Gabrielyan, V. Fromzel, and M. Dubinskii, "Linear thermal expansion and thermo-optic coefficients of YVO4 crystals the 80-320 K temperature range," *Opt. Mater. Express*, vol. 2, no. 11, pp. 1624–1631, Oct. 2012.
14. I. Dolev, A. Ganany-Padowicz, O. Gayer, A. Arie, J. Mangin, and G. Gadret, "Linear and nonlinear optical properties of MgO:LiTaO3," *Appl. Phys. B.*, vol. 96, no. 2–3, pp. 423–432, Apr. 2009.
15. G. Baili, F. Bretenaker, M. Alouini, L. L. Morvan, D. Dolfi, and I. Sagnes, "Experimental Investigation and Analytical Modeling of Excess Intensity Noise in Semiconductor Class-A Lasers," *J. Light. Technol.*, vol. 26, no. 8, pp. 952–961, 2008.
16. G. J. Dick, "Local oscillator induced instabilities in trapped ion frequency standards," in *Proc. 19th Precise Time and Time Interval (PPTI) Applications and Planning Meeting*, 1987, pp. 133–147.